ASTFE American Society of Thermal and Fluids Engineers

5th-6th Thermal and Fluids Engineering Conference (TFEC)
May 26-28, 2021
Virtual Conference

TFEC-2020-36291

LOOP THERMOSYPHON DESIGN FOR SOLAR THERMAL DESALINATION

Joshua Charles[1*], Nathan Van Velson[1]

[1]Advanced Cooling Technologies, 1046 New Holland, Ave. Lancaster, PA 17601, USA

ABSTRACT

A two-phase loop thermosyphon solar collector is under development that can efficiently and passively transfer thermal energy from a concentrated solar collector to a thermal desalination process. The design of a loop thermosyphon is critical to ensure that the thermosyphon can transfer the required thermal energy through the passive circulation of a two-phase flow. This flow is driven by the difference in gravitational head between the liquid return line and the two-phase riser located between the evaporator and condenser. A numerical mass, energy, and pressure balance model was developed to provide insights into the behavior of the two-phase working fluid and predict system performance as geometric parameters (tube diameter, condenser height, etc.) are varied. This model is based on well-established empirical two-phase pressure drop and heat transfer correlations. The model accounts for gravitational head and frictional, minor, and acceleration pressure drops throughout and uses locally-calculated heat transfer coefficients to estimate heat losses and heat exchanger performance. A lab-scale loop thermosyphon prototype has been tested across a range of fluid charges, saturation temperatures, and evaporator powers. Modeling results for flow rate and pressure drop have been found to agree well with experimental data across the range of conditions examined. This model is a valuable tool to design and optimize a wide range of two-phase loop thermosyphons for solar thermal and other heat transfer applications.

KEYWORDS: Loop Thermosyphon, Solar Desalination, Pressure Drop Modeling, Heat Transfer, Two-Phase Flow

1. INTRODUCTION

There has been an increased focus on utilizing concentrated solar power (CSP) for thermal desalination. CSP is an attractive option for providing heat to a desalination process as the intermittency of solar irradiance is countered by the ability to easily store the purified water. Moreover, the high energy requirement of thermal desalination is countered by the use of the renewable and free supply of solar energy. State-of-the-art (SOTA) CSP systems typically utilize parabolic trough solar concentrators coupled with steel evacuated tube receivers. In this configuration, the CSP system experiences optical losses across the trough and transmittance and heat transfer losses within the receiver. There are further system losses due to heat transfer losses from the field tubing and parasitic power demands – primarily the heat transfer fluid (HTF) pumping power. Advanced Cooling Technologies (ACT) has designed a solar thermal desalination system with a novel solar receiver and HTF. This system is designed around a two-phase loop thermosyphon (LTS), which eliminates the need for a pump. The design of ACT's thermal desalination system is presented in Fig. 1.

The thermal desalination system developed by ACT improves the SOTA in several key ways. At the solar absorptance level, the steel receiver tube has been replaced by a vacuum insulated glass receiver tube. This allows incident solar irradiance to pass directly through the tube and be volumetrically absorbed within the working fluid instead of on the outer surface of the tube. This change eliminates thermal resistance through the tube wall. To achieve volumetric absorption, the working fluid must be tuned to absorb virtually all of the incident radiation across the entire solar spectrum. This working fluid must remain stable during repeated heating and cooling cycles and not degrade during prolonged UV exposure. ACT is currently evaluating the

*Corresponding Author: josh.charles@1-act.com

long-term stability of several promising working fluids. Modeling suggests that the use of a glass receiver with volumetric absorption working fluid has the potential to increase the solar to thermal conversion efficiency by around 2% absolute.

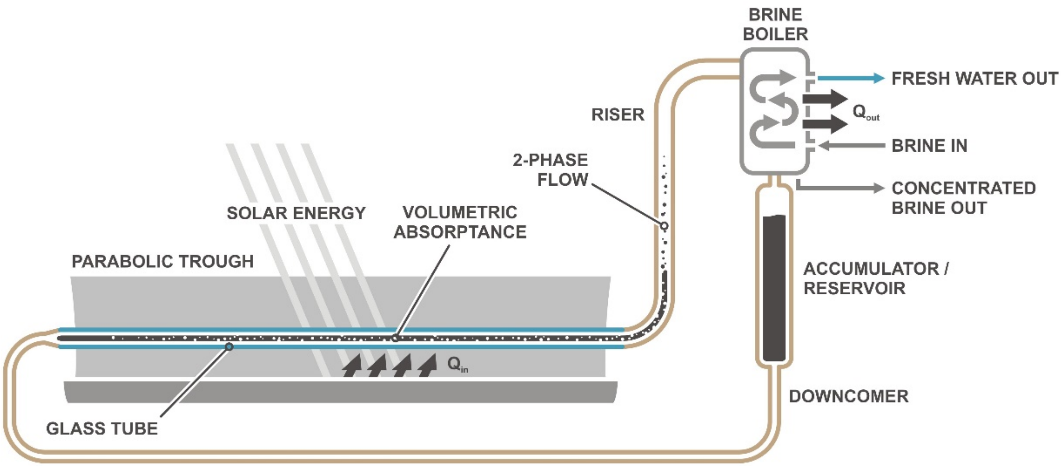

Fig. 1 Design of a concentrated solar loop thermosyphon for thermal desalination developed by Advanced Cooling Technologies.

A more significant improvement on the SOTA is the use of a two-phase working fluid between the solar receiver and brine heater. A two-phase working fluid offers several benefits over a single-phase fluid. First, by storing thermal energy using the latent heat of vaporization, a larger quantity of thermal energy can be transferred at a reduced working fluid temperature and flow rate. A lower fluid temperature reduces thermal losses to the environment between the receiver and brine boiler. Two-phase flow also results in increased heat transfer rates within the brine boiler, where the working fluid condenses. The higher condensation heat transfer coefficient allows for the surface area (i.e., size) of the brine boiler to be reduced, decreasing system capital costs. However, the greatest benefit of two-phase flow is that it allows the system to passively operate as a loop thermosyphon, eliminating the need for a pump. Turton et al. [1] suggest a present-day pump cost of $2,337/kW for a centrifugal pump. A pump lifetime of 15 years and a 3% discount rate were assumed. The pump was found to account for ~19% of the total levelized cost of heat (LCOH) of a SOTA solar desalination system. By utilizing a passive loop thermosyphon, the pump can be removed, eliminating this cost.

2. LOOP THERMOSYPHON OPERATION

A thermosyphon is a variation of a heat pipe, where the condensate is returned to the evaporator by gravity. The operation of a traditional single-tube thermosyphon is presented in Fig. 2 (a). Heat is applied to the bottom of the thermosyphon, where the working fluid boils. Vapor rises against gravity from the evaporator to the condenser. As heat is removed from the vapor in the condenser, the vapor condenses and falls back to the evaporator along the wall of the thermosyphon. The maximum power of a thermosyphon is limited by the flooding limit, which is imposed by shear forces between the high-velocity upward flowing vapor and the downward flowing liquid [2]. A loop thermosyphon (LTS) bypasses the flooding limit by separating the liquid and vapor lines, eliminating shear between the phases. LTS operation is illustrated in Fig. 2 (b).

Like a traditional thermosyphon, heat is applied in an evaporative zone at the bottom of the loop, with vapor rising along a riser to the condensation zone at the top of the system. Heat is removed from the working fluid in the condensation zone, condensing the working fluid, which returns to the evaporator via the liquid return line. A unique feature of an LTS is its ability to push a two-phase vapor/liquid flow from the evaporator to the condenser. The force required to lift the denser two-phase (2ϕ) flow is provided by the gravitational head of the liquid column beneath the condenser ($\Delta P_{g\ liq}$). This gravitational head is resisted by the head of the two-phase fluid in the riser ($\Delta P_{g\ 2\phi}$), the frictional pressure drop along the liquid portion of the loop ($\Delta P_{f\ liq}$), and the frictional pressure drop along the two-phase portion of the loop ($\Delta P_{f\ 2\phi}$). There are also pressure drops associated with changes in momentum around the loop ($\Sigma\Delta P_a$) and minor losses around elbows and through fittings ($\Sigma\Delta P_m$). These six pressure components are in balance during steady-state operation, a fact that forms the basis for the LTS modeling presented in this report:

$$\Delta P_{g\,liq}+\Delta P_{g\,2\phi}+\Delta P_{f\,liq}+\Delta P_{f\,2\phi}+\sum\Delta P_a+\sum\Delta P_m=0 \quad (1)$$

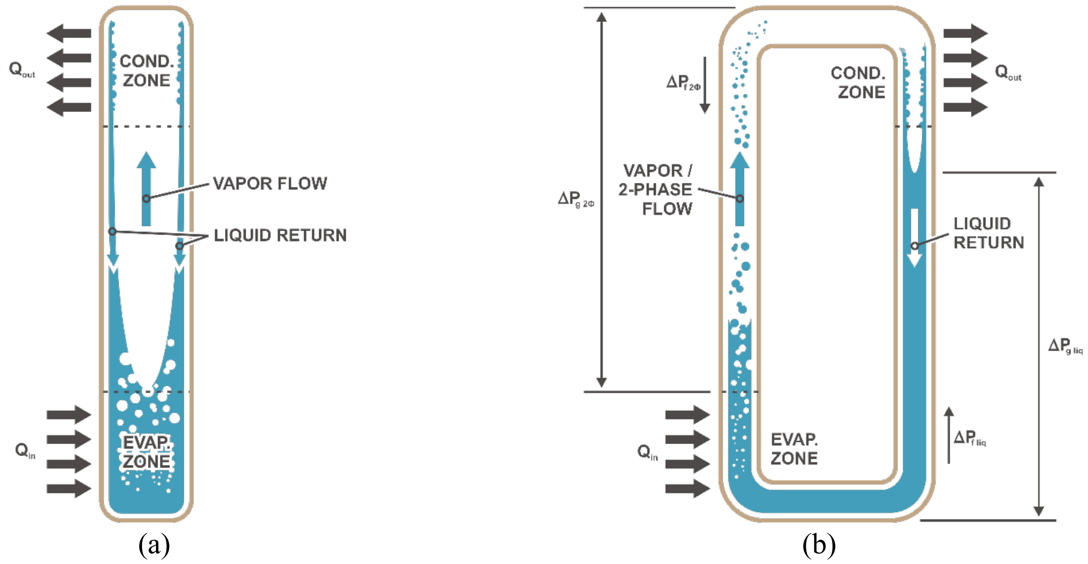

Fig. 2 (a) Operation of a traditional thermosyphon where the vapor and liquid flow along the same tube vs. (b) a loop thermosyphon where the vapor or two-phase fluid and liquid return flow along separate tubes.

Many researchers have examined the performance of loop thermosyphons both empirically and through detailed modeling efforts. Qu [3] and Sai Sudheer et al. [4] used the conservation of momentum, continuity, and heat transfer equations to calculate the performance of each section of the loop. However, their work focused on a single-phase vapor riser, and Sai Sudheer et al. assumed a point-source evaporator and condenser. Hartenstine et al. [5] conducted a numerical analysis of a two-phase loop thermosyphon using the two-phase pressure drop correlation by Lockhart and Martinelli [6]. This work demonstrated a model similar to the present work, but it was limited to a single geometry and the modeling results were not compared against equivalent experimental data. Lockhart and Martinelli's (L-M) work has formed the basis for many two-phase frictional pressure drop correlations. Chisholm presented a refinement on the L-M model [7]. Silva et al. [8] and Yadav [9] proposed a refinement on the L-M model to account for the two-phase minor losses through elbows. In addition to the L-M correlation, Bankoff [10], Cavallini et al. [11], Chisholm [12], Fiedel [13,14], and Ghajar et al. [15,16] have all proposed two-phase frictional pressure drop correlations for straight tube flow. Each correlation is best suited to specific flow orientations, flow regimes, and working fluids, making the implementation of a universal model difficult. The present work navigates this challenge by incorporating each of these frictional pressure drop correlations into the model, with the correlation used being user-selectable based on the flow characteristics and fluid. Unlike some previous modeling work, the present model was validated against experimental data from a geometrically-equivalent loop thermosyphon.

4. THE LOOP THERMOSYPHON MODEL

A model capable of predicting the performance of various LTS geometries was developed using the pressure balance presented in Equation (1). This 1D, steady-state model divides the LTS into discrete sections, which are sequentially operated on. There are 4 primary types of sections defined within the model: evaporator, condenser, tube, and elbow sections. A visual representation of the model discretization is presented in Fig. 3. For each section, critical dimensions (diameters, length, inclination, elbow radius, etc.) are user input and are used to define the LTS geometry. Other required model inputs are the working fluid, the saturation temperature, operating temperature, and fluid quality at the entrance or exit of one of the sections. The point at which this information is entered forms the starting point of the 1D numerical analysis.

Upon execution, the model first uses the specified temperatures and quality to calculate the fluid enthalpy and pressure at the specified starting section. Enthalpy and pressure are base-level fluid parameters of the model. The reason for this is that the energy and pressure drop balance can be fully described using only these two values, greatly simplifying the calculation routine. All other fluid properties (temperature, density, viscosity, surface tension, quality, etc.) are derived from the base fluid parameters as required during model execution.

After the model executes at the specified starting point, the pressure drop and heat transfer for the starting section is calculated, with the results of this analysis used to predict the pressure and enthalpy of the fluid at the exit of the starting section. After writing these values to the input of the next downstream section, the model serially executes the pressure and energy balance for each section around the loop. The model continues around the loop until the difference in pressure and enthalpy between subsequent loops falls below a specified tolerance.

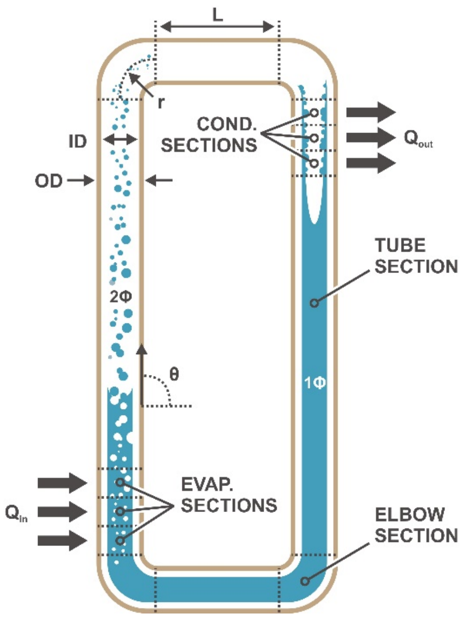

DIMENSIONS
- ID: Inner Diameter
- OD: Outer Diameter
- L: Length
- A: Cross-sectional Area
- θ: Tube Inclination (relative to the positive x-axis)
- r: Elbow Radius

BASE FLUID PARAMETERS
- h: Enthalpy
- P: Pressure

DERIVATIVE FLUID PARAMETERS
- T: Temperature
- ρ: Density
- μ: Viscosity
- σ: Surface Tension

CALCULATED FLUID PARAMETERS
- ΔP_f: Frictional Pressure Drop
- ΔP_g: Gravitational Head
- ΔP_a: Acceleration Pressure Drop
- ΔP_m: Minor Pressure Losses
- α: Void Fraction
- h_c Convective Heat Transfer Coefficient

Fig. 3 LTS model discretization scheme and specified critical dimensions and fluid parameters. The model converges on the base fluid parameters, with derived fluid parameters calculated from these base parameters. Pressure drop and heat transfer correlations within the model are used to predict the calculated fluid parameters.

Outputs from the model include complete frictional, gravitational, acceleration, and minor pressure losses for each section as well as complete temperature and pressure profiles and the calculated sectional fluid qualities and void fractions. Convective heat transfer coefficients between the fluid and inner surface of the tube are calculated and used to estimate thermal losses to the environment. The model also predicts the fluid mass flow rate and the fluid charge of the system.

5. FRICTIONAL PRESSURE DROP CORRELATIONS

Accurate calculation of frictional pressure losses around the loop is critical to the accuracy of the 1D numerical model. For single-phase sections (fully liquid or vapor), frictional pressure drop is calculated using the standard Darcy friction factor equation for tubular flow. However, this method does not apply to the two-phase flow in the evaporator, riser, or condenser. Two-phase flow pressure drop is highly complex due to the turbulent nature of two-phase flow and the many possible flow regimes (annular, bubbly, churn, etc.) which occur at different void fractions, velocities, and flow orientations. Because of this, the two-phase frictional pressure drop is typically calculated using empirically-derived correlations. Several two-phase frictional pressure drop correlations are widely accepted as having a good agreement with empirical data across a range of flow regimes. Arguably, the most popular of these correlations was first proposed by Lockhart and Martinelli (L-M) in 1949 [6]. The L-M, and most other correlations, utilize a two-phase frictional pressure drop multiplier

($\phi_j^{2\phi}$), which is multiplied by the single-phase frictional pressure drop for either the liquid (subscript $_l$) or vapor (subscript $_g$) portions of the flow:

$$\left(\frac{dP_f}{dz}\right)^{2\phi} = \phi_l^{2\phi}\left(\frac{dP_f}{dz}\right)_{liq} = \phi_g^{2\phi}\left(\frac{dP_f}{dz}\right)_{gas} \tag{2}$$

Some correlations calculate the single-phase pressure drop assuming the entire fluid flow is flowing as liquid only (subscript $_{lo}$), leading to a similar equation for the two-phase pressure drop based on the liquid only frictional pressure drop and a liquid-only two-phase multiplier ($\phi_{lo}^{2\phi}$).

$$\left(\frac{dP_f}{dz}\right)^{2\phi} = \phi_{lo}^{2\phi}\left(\frac{dP_f}{dz}\right)_{liq} \tag{3}$$

Six well-documented two-phase frictional pressure drop correlations are presented in Table 1. Each of these correlations uses fluid flow conditions to solve for a liquid or liquid only two-phase multiplier, which is used to find the two-phase pressure drop using either Equation (2) or (3). All of the correlations presented in Table 1 are implemented and user-selectable within the LTS model user interface.

Table 1 Summary of the two-phase pressure drop correlations implemented in the sectional LTS model

Source	Correlation Equations and Variables
[6]	$\Phi_l^2 = 1 + \frac{C}{X} + \frac{1}{X^2}$; $X = \sqrt{\frac{\left(\frac{dP_f}{dz}\right)_l}{\left(\frac{dP_f}{dz}\right)_g}}$; C = 5: lam-lam flow, C = 10: lam-turb, C = 12: turb-lam, C = 20: turb-turb
[10]	$\Phi_l^2 = \left(\left(\frac{1}{1-x}\right)\left(1-\Gamma_{Bf}\left(1-\frac{\rho_g}{\rho_l}\right)\right)^{0.43}\left(1+x\left(\frac{\rho_g}{\rho_l}-1\right)\right)\right)^{1.75}$; $\Gamma_{Bf} = \left(\frac{0.71+2.35\left(\frac{\rho_g}{\rho_l}\right)}{1+\left(\frac{1-x}{x}\right)\left(\frac{\rho_g}{\rho_l}\right)}\right)$
[11]	$\Phi_{lo}^2 = A_{Fr} + \frac{1.262x^{0.6978}}{We_{go}^{0.1458}}\left(\frac{\rho_l}{\rho_g}\right)^{0.3278}\left(\frac{\mu_g}{\mu_l}\right)^{-1.181}\left(1-\frac{\mu_g}{\mu_l}\right)^{3.477}$; $A_{Fr} = (1-x)^2 + x^2\left(\frac{\rho_l}{\rho_g}\right)\left(\frac{f_{go}}{f_{lo}}\right)$
[12]	$\Phi_{lo}^2 = 1 + (Y^2-1)\left(B_{CH}x^{(1-0.5n)}\left(1-x^{(1-0.5n)}\right)\right) + x^{(2-n)}$; n = 0.25; $Y^2 = \frac{\left(\frac{dP}{dL}\right)_{go}}{\left(\frac{dP}{dL}\right)_{lo}}$ $0 \le Y \le 9.5$: $G \le 500$: $B_{CH} = 4.8$; $500 < G < 1900$: $B_{CH} = 2400/G$; $1900 \le G$: $B_{CH} = 55/\sqrt{G}$ $9.5 < Y \le 28$: $G \le 600$: $B_{CH} = 520/\sqrt{Y^2G}$; $600 < G$: $B_{CH} = 21/Y$ $28 < Y$: $B_{CH} = 15000/\left(Y^2\sqrt{G}\right)$
[13,14]	$For\ \theta = 0°\ or\ +90°$: $\Phi_{lo}^2 = A_{Fr} + \frac{3.24x^{0.78}(1-x)^{0.22}(\rho_l/\rho_g)^{0.91}(\mu_g/\mu_l)^{0.19}\left(1-(\mu_g/\mu_l)\right)^{0.7}}{Fr_{lo}^{0.045}We_{lo}^{0.035}}$ $For\ \theta = -90°$: $\Phi_{lo}^2 = A_{Fr} + \frac{5.7x^{0.7}(1-x)^{0.14}(\rho_l/\rho_g)^{0.85}(\mu_g/\mu_l)^{0.36}\left(1-(\mu_g/\mu_l)\right)^{0.2}}{Fr_{lo}^{0.09}We_{lo}^{0.007}}$ $f_{lo} = 0.25\left(0.86859\ ln\left(\frac{Re_l}{1.964\ ln(Re_l)-3.8215}\right)\right)^{-2}$; $f_{go} = 0.25\left(0.86859\ ln\left(\frac{Re_g}{1.964\ ln(Re_g)-3.8215}\right)\right)^{-2}$ $Fr_{lo} = \frac{G^2}{gd_h\rho_l^2}$; $We_{lo} = \frac{G^2d_h}{\sigma\rho_l}$; $A_{Fr} = (1-x)^2 + x^2\left(\frac{\rho_l}{\rho_g}\right)\left(\frac{f_{go}}{f_{lo}}\right)$
[15,16]	$\Phi_{lo}^2 = 1 + dP_{Fr}\left[\frac{\left(\frac{\rho_l}{\rho_g}\right)}{\left(\frac{\mu_l}{\mu_g}\right)^{0.25}} - 1\right]$; $dP_{Fr} = f_{Fr}\left(x + 4\left(x^{1.8} - x^{10}f_{Fr}^{0.5}\right)\right)$; $Fr_{lo} = \frac{G^2}{gd_h\rho_l^2}$ $Fr_{lo} \ge 1$: $f_{Fr} = 1.0$; $Fr_{lo} < 1$: $f_{Fr} = Fr_{lo}^{0.3} + 0.0055\left(ln\left[\frac{1}{Fr_{lo}}\right]\right)^2$

In addition to an accurate estimation of two-phase pressure drop, an accurate prediction of the two-phase void fraction is critical to estimating the system fluid charge and heat transfer characteristics. Fifteen well-documented void fraction estimation correlations have also been implemented in the model [15]. Before model execution, the user selects both the frictional pressure drop and void fraction method to be used.

6. HEAT TRANSFER METHODS

Methods for calculating the boiling, two-phase, and condensation heat transfer coefficients are needed for accurate predictions of heat transfer within the evaporator and condenser as well as heat losses throughout the loop. Kandlikar proposed a correlation for predicting the saturated flow boiling heat transfer coefficient ($h_{2\phi b}$) as a function of the convective (Co) and boiling (Bo) numbers, the single-phase heat transfer coefficient (h_{liq}), a fluid parameter (F_{fl}), the liquid only Froude number (Fr_{lo}), and five constants (C_1-C_5):

$$h_{2\phi b} = C_1 Co^{C_2}(25Fr_{lo})^{C_5} h_{liq} + C_3 Bo^{C_4} h_{liq} F_{fl} \tag{4}$$

Methods for the calculation of these variables and constants can be found in the paper by Kandlikar [17]. For two-phase regions not dominated by boiling or condensation, Chen's modified Dittus-Boelter equation is used to find the two-phase heat transfer coefficient ($h_{2\phi}$) [18]:

$$h_{2\phi} = 0.023(Re_m)^{0.8}(Pr_l)^{0.4}\frac{k_l}{d_h} \tag{5}$$

Where Re_m is the Reynolds number of the homogeneous two-phase mixture. Within the condenser, the condensation two-phase heat transfer coefficient ($h_{2\phi c}$) is estimated using Shah's correlation for vertical, inclined, or horizontal condensers as presented by Papini et al. [19].

$$h_{2\phi c} = h_l\left[(1-x)^{0.8} + \frac{3.8x^{0.76}(1-x)^{0.04}}{Pr_l^{0.38}}\right] \tag{6}$$

Within the single-phase liquid region, a Dittus-Boelter equation was used to solve for the single-phase liquid heat transfer coefficient (h_l). Heat loss from each section was estimated using a thermal resistance network beginning at the fluid/tube interface and ending at the interface between the insulation surrounding the tube and the ambient air.

7. LAB-SCALE SOLAR THERMAL-DRIVEN LOOP THERMOSYPHON

The pressure drop and heat transfer LTS model was used to design a lab-scale loop thermosyphon with a configuration similar to that of a future full-scale solar-heated LTS. Initially, the working fluid is heated in a horizontal evaporator using 10 resistive band heaters. These heaters simulate heating by a concentrated solar source. In the near future, the copper tube and band heaters will be replaced by a glass tube, which will allow the system to be heated by a solar simulator, with a parabolic trough used to concentrate the rays. After exiting the evaporator, the two-phase working fluid rises vertically to a flat plate condenser where it is condensed by a metered chilled water loop. The geometry of this system is presented in Fig. 4 (a). The 1-meter long evaporator is located approximately 0.5 m below the condenser, with the evaporator and two-phase riser having an inner diameter (ID) of 25 mm and the downcomer and liquid return line, 19 mm. A 50 mm ID accumulator was added to the upper portion of the downcomer to serve as a working fluid reservoir and to damp oscillations of the liquid head in the liquid return line. Since the downcomer liquid head provides the working fluid motive force, oscillations in this head can lead to significant transient flow instabilities around the loop.

The final design for the lab-scale LTS with solar simulator is presented in Fig. 4 (b). The copper, resistively-heated evaporator will be replaced with a borosilicate glass tube with columnar light from three 2,500W metal halide lamps concentrated onto the tube via a parabolic trough.

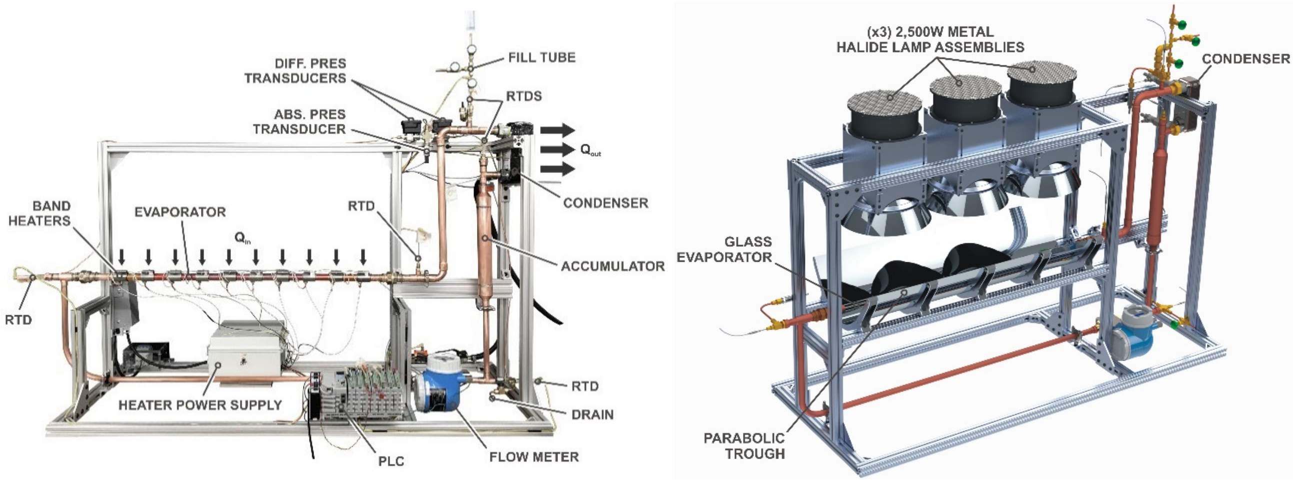

(a) (b)

Fig. 4 (a) The constructed lab-scale LTS prototype with instrumentation and controls and (b) the design of the lab-scale prototype with a 3-lamp solar simulator and parabolic trough concentrator.

Before constructing the lab-scale prototype, the LTS model was used to verify system performance. The LTS was designed for operation between 1 and 2.5 kW at saturation temperatures between 110 and 130°C. System operation across this range of operating conditions was predicted using the L-M pressure drop and void fraction correlations within the sectional LTS model. The predicted mass flow rate vs. power for 110, 120, and 130°C is presented in Fig. 5 (a).

Fig. 5 (a) suggests that at each operating temperature, the flow rate will initially increase with power before peaking and falling at higher powers. As seen in Fig. 5 (b) void fraction is predicted to increase linearly across the power range considered. The increasing void fraction initially increases the flow rate as the density of the two-phase flow in the riser decreases. However, as void fraction increases further, the increase in two-phase frictional pressure drop begins to dominate. Eventually, the decrease in the two-phase head is completely offset by the increase in two-phase frictional pressure drop and this point corresponds to the peak mass flow rate seen in Fig. 5 (a).

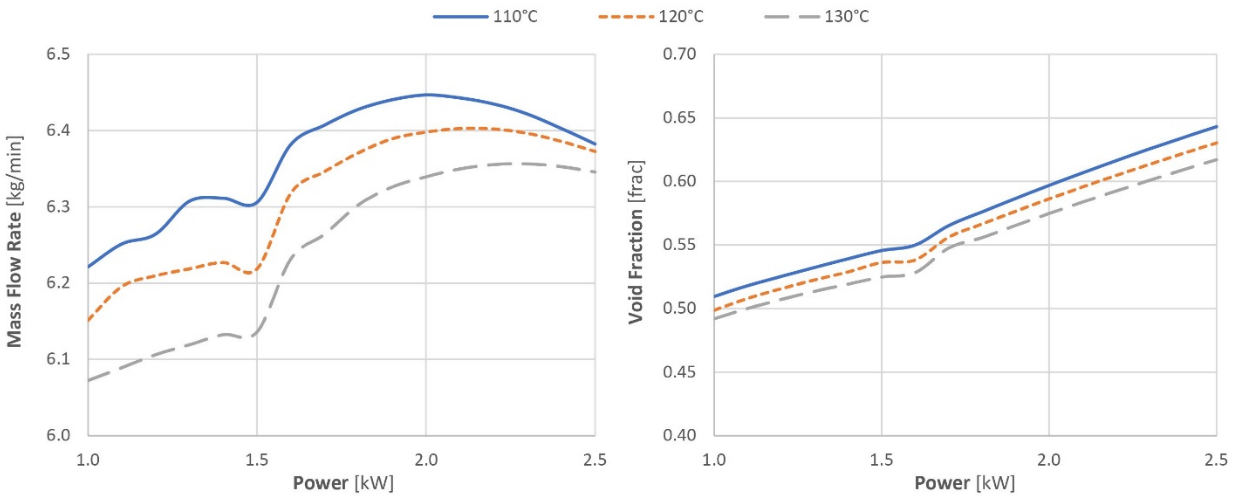

(a) (b)

Fig. 5 (a) Modeled mass flow rate and (b) void fraction for the lab-scale LTS system designed by ACT. For all cases, the operating fluid liquid head was assumed to reach exactly to the exit of the condenser.

The constructed lab-scale LTS was tested at evaporator powers between 1 and 2.5 kW and two-phase fluid temperatures of 110 and 120°C. RTDs were used for temperature measurements of the fluid entering and leaving the evaporator and condenser with absolute pressure transducers used for pressure measurement at the evaporator inlet, condenser inlet, and bottom of the liquid return line. The working fluid flow rate was measured by an electromagnetic flowmeter in the liquid return line. The condenser was cooled by a metered cooling water loop supplied by an industrial chiller. Instrumentation and system control were handled by a programable logic controller (PLC). The system was leak tested under vacuum before being charged with between 1,650 and 1,750 ml of deionized water. For each test charge, power, and temperature the system was operated at steady-state for 5 to 10 minutes, with the experimental data values averaged across this steady-state time. An example of the instantaneous temperature data reported during a 110°C steady-state test is presented in Fig. 6 (a). While there is a periodic fluctuation in temperature (on the order of 200 seconds), the variations are consistent and repeatable, allowing the data to be averaged to provide representative steady-state values for each test period.

In addition to temperature data, the fluid mass flow rate was recorded during each test [see example test in Fig. 6 (b)]. Taken alone, mass flow rate provides little information about the thermal operation of the LTS, but since mass flow rate is a function of pressure drop, it can be directly used to compare the experimental system performance to that predicted by the model. The thermal energy removed in the condenser and the subcooling of the working fluid across the condenser were used to calculate the quality of the two-phase fluid entering the condenser. While quality cannot be directly equated to the two-phase void fraction due to slip between the liquid and vapor phases, it is still an indicator of the percentage of flow vaporized and condensed during each circuit of the loop.

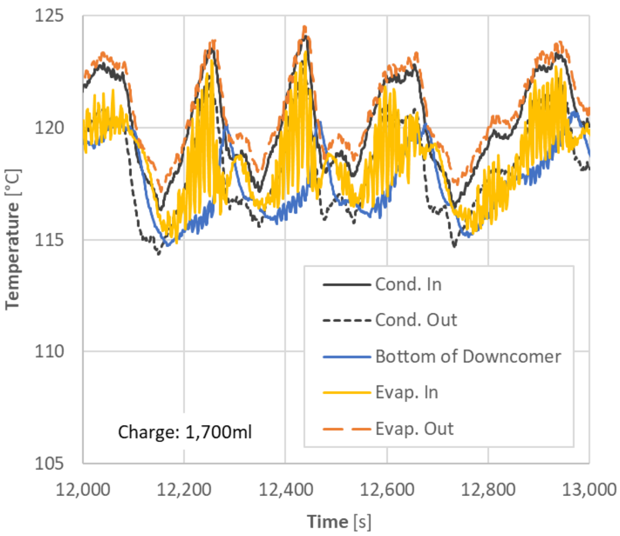

(a)

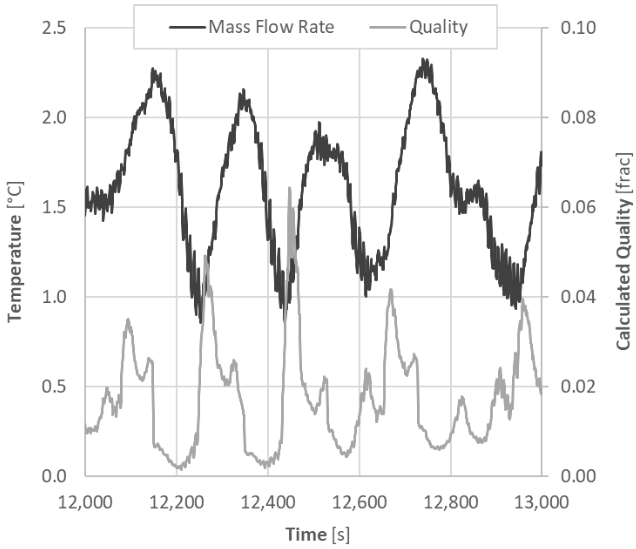

(b)

Fig. 6 (a) Transient temperature data for one of the steady-state LTS tests and (b) Transient mass flow rate and calculated two-phase quality for the same steady-state LTS test.

Experimental (EXP) and modeling (MOD), steady-state flow rate results for the lab-scale LTS are presented in Fig. 7 (a) for 1,650 and 1,750 ml fluid charges and saturation temperatures of 110 and 120°C. The modeling results were produced using the L-M pressure drop correlation implemented in the model. For all charges and temperatures, increasing evaporator power was found to correlate to an increase in working fluid flow. This is expected as the thermal energy input to the system directly drives the flow through the density reduction of the two-phase working fluid. The trend of increasing flow rate with increasing power was observed in both the experimental and model results. Also, the flattening of the experimental flow rate trend at powers greater than ~2,000W is observed in nearly all of the modeling result curves. The difference between model and experiment is visualized in Fig. 7 (b), where modeled mass flow rate is plotted against experimental mass flow rate. This plot shows that for the temperatures and charges considered, the model, on average, overpredicts mass flow rate by between 20 and 30%. While this difference is significant, it is within the typical error associated with the L-M correlation due to the highly complex nature of two-phase flow regimes. Additional work is being conducted to determine the specific mechanisms responsible for this difference between model and experiment and propose improvements to the correlations used.

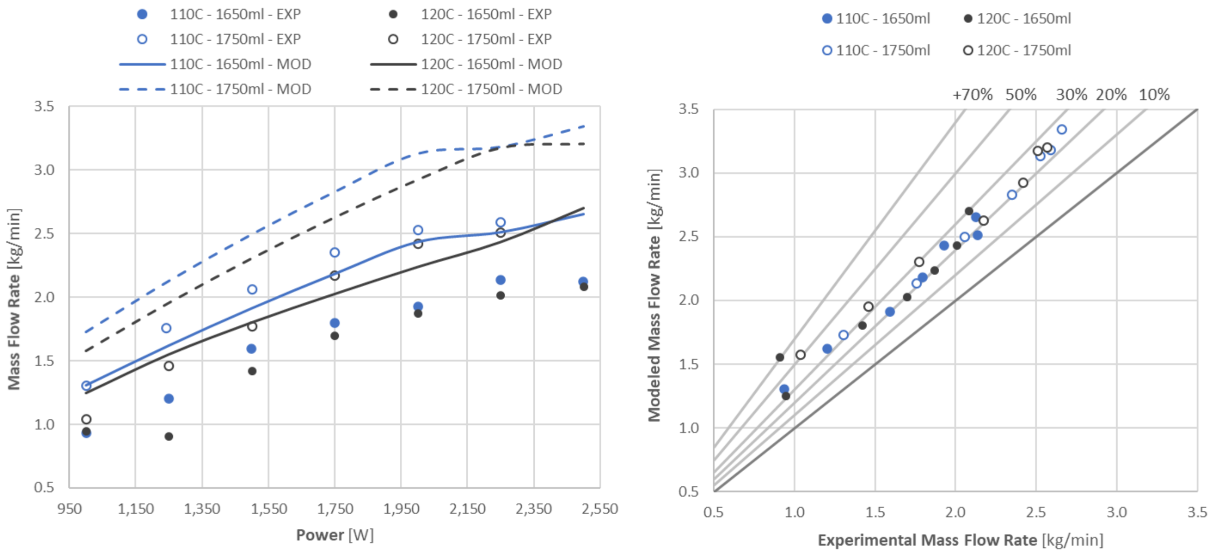

(a) (b)

Fig. 7 (a) Modeling and experimental LTS mass flow rate results vs. evaporator power at 110 and 120°C and 1,650 and 1,750ml of charge and (b) the difference in modeled and experimental mass flow rate for the lab-scale LTS.

8. CONCLUSIONS

This work demonstrated that the new, sectional LTS model can predict the performance of the solar desalination LTS under development at ACT. While a mass flow rate difference was found between the experimental and model results, the differences were within the prediction uncertainty of the two-phase Lockhart and Martinelli pressure drop correlation used in the model. Similar modeling with other pressure drop correlations (beginning with those presented in Table 1) is planned to explore which correlation has the best prediction capabilities for the present LTS configuration and working fluid.

The next experimental step will be to replace the lab-scale LTS's resistively-heated evaporator with a transparent glass tube with thermal energy supplied by three metal halide solar simulators. A parabolic trough placed beneath the tube will concentrate the incident rays onto the highly absorptive working fluid flowing through the glass evaporator.

ACKNOWLEDGMENTS

This work was performed for the Solar Energy Technology Office (SETO) under contract number DE-EE000839. The technical monitor is Mark Lausten. The authors would like to acknowledge Adam Shreve for his assistance in the design, assembly, and testing of the lab-scale loop thermosyphon.

NOMENCLATURE

2ϕ	Two-phase flow		T	Fluid temperature	(°C)
ΔP	Pressure drop	(Pa)	ρ	Fluid density	(kg/m^3)
ID	Inner tube diameter	(m)	μ	Fluid viscosity	(Pa-s)
OD	Outer tube diameter	(m)	σ	Fluid surface tension	(N/m)
L	Section length	(m)	α	Fluid void fraction	
A	Section cross-sectional area	(m^2)	x	Fluid quality	
θ	Tube inclination	(°)	G	Mass flux ($\dot{m}$/A)	(kg/s-m^2)
r	Elbow radius	(m)	f	Friction factor	
h	Fluid enthalpy	(kJ/kg)	h_c	Convective heat trans. coeff.	(W/m^{2}K)
P	Fluid pressure	(Pa)	ϕ_j	Two-phase pressure drop mult.	

d_h	Hydraulic diameter	(m)	*liq*	Liquid phase
Co	Convective number		*gas*	Vapor phase
Bo	Boiling number		*f*	Frictional pressure drop
F_{fl}	Kandlikar fluid parameter		*a*	Acceleration pressure drop
Fr	Froude number		*m*	Minor pressure losses
C_i	Kandlikar constants		*l*	Liquid portion of total flow
Re_m	Mixture Reynolds number		*g*	Vapor portion of total flow
Pr	Prandtl number		*lo*	Liquid only flow
			go	Vapor only flow
Subscripts			*b*	Boiling flow
g	Gravitational head		*c*	Condensing flow

REFERENCES

[1] Turton, R., Bailie, R., Whiting, W., Shaeiwitz, J.A., Bhattacharyya, D. Analysis, Synthesis, and Design of Chemical Processes. 4th Edition. Prentice Hall, (2013).
[2] Advanced Cooling Technologies. "Loop Thermosyphon." Accessed 3/10/2021 from <https://www.1-act.com/resources/heat-pipe-fundamentals/different-types-of-heat-pipes/thermosyphons/loop-thermosyphon/>
[3] Qu, W. "Hydrodynamics of Two-Phase Loop Thermosyphon." *Frontiers in Heat Pipes, 1*, 023004, (2010).
[4] Sai Sudheer, S., Kiran Kumar, K., Balasubramanian, K., Babu B., R. "Steady State Performance of Two Phase Natural Circulation Loop: Two Vertical Branches with Point Heat Source and Sink." *International Journal of Advanced Trends in Computer Applications,*1(1), pp. 55-59, (2019).
[5] Hartenstine, J., Bonner, R., Montgomery, J., Semenic, T. "Loop Thermosyphon Design for Cooling of Large Area, High Heat Flux Sources." *Proceedings of IPACK2007*, Vancouver, British Columbia, Canada, July 2007.
[6] Lockhart, R. W., Martinelli, R. C. "Proposed Correlation of Data for Isothermal Two-Phase Two-Component Flow in Pipes," Chemical Engineering Progress, 45(1), pp. 39-48, (1949).
[7] Chisholm, D. "A Theoretical Basis for the Lockhart-Martinelli Correlation for Two-Phase Flow," *International Journal of Heat and Mass Transfer, 10*, pp. 1767-1778, (1967).
[8] Silva, S., Resendiz, L., Mariscal, C., Eslava, T. "Pressure Drop Models Evaluation for Two-Phase Flow in 90 Degree Horizontal Elbows." Ingeniería Mecánica Tecnología Y Desarrollo, 3(4), pp. 115-122, (2010).
[9] Yadav, M. S. "Interfacial Area Transport Across Vertical Elbows in Air-Water Two-Phase Flow," PhD thesis, Pennsylvania State University, (2013).
[10] Bankoff, S. G. "A Variable Density Single Fluid Model for Two Phase Flow with Particular Reference to Steam-Water Flow." *J. Heat Transfer,* 11, pp. 165–172, (1960).
[11] Cavallini, A., Censi, G., Del Col, D., Doretti, L., Longo, G.A., Rossetto, L. "Condensation of Halogenated Refrigerants Inside Smooth Tubes." HVAC&R Res. 8, pp. 429–451 (2002).
[12] Chisholm, D. "Pressure Gradients Due to the Friction During the Flow of Evaporating Two Phase Mixtures in Smooth Tubes and Channels." Int. J. Heat Mass Transf. 16, pp. 347–358 (1973).
[13] Friedel, L. "Improved Friction Pressure Drop Correlation for Horizontal and Vertical Two Phase Pipe Flow." Eur. Two Phase Flow Group Meet. Pap. 18, pp. 485–492 (1979).
[14] Friedel, L. "Two-Phase Frictional Pressure Drop Correlation for Vertical Downflow." Ger. Chem. Eng. 8(1), pp. 32–40 (1985).
[15] Ghajar, A., Bhagwat, S. "Chapter 4: Flow Patterns, Void Fraction and Pressure Drop in Gas-Liquid Two Phase Flow at Different Pipe Orientations." Frontiers and Progress in Multiphase Flow 1, Cheng, L. (ed.). Springer International Publishing, Switzerland, (2014).
[16] Wolverine Tube, Inc. "Chapter 13: Two-Phase Pressure Drops." Accessed 12/8/2020 from <http://www.thermalfluidscentral.org/e-books/pdf/edb3/13.pdf>, (2006).
[17] Kandlikar, S. G. "A General Correlation for Saturated Two-Phase Flow Boiling Heat Transfer Inside Horizontal and Vertical Tubes," in *Journal of Heat Transfer, 112,* pp. 219-228, (1990).
[18] Chen, J. C. "A Correlation for Boiling Heat Transfer to Saturation Fluids in Convective Flow," Brookhaven National Laboratory, Upton, NY, (1962).
[19] Papini, D., Cammi, A. "Modeling of Heat Transfer Phenomena for Vertical and Horizontal Configurations of In-Pool Condensers and Comparison with Experimental Findings," in *Science and Technology of Nuclear Installation,* (2010).